The Astrophysical Journal Supplement Series, 173:256–266, 2007 December

EXTINCTION-CORRECTED STAR FORMATION RATES EMPIRICALLY DERIVED FROM ULTRAVIOLET–OPTICAL COLORS

Marie Treyer,[1,2] David Schiminovich,[3] Ben Johnson,[3] Mark Seibert,[4] Ted Wyder,[2] Tom A. Barlow,[2] Tim Conrow,[2] Karl Forster,[2] Peter G. Friedman,[2] D. Christopher Martin,[2] Patrick Morrissey,[2] Susan G. Neff,[5] Todd Small,[2] Luciana Bianchi,[6] José Donas,[1] Timothy M. Heckman,[7] Young-Wook Lee,[8] Barry F. Madore,[4] Bruno Milliard,[1] R. Michael Rich,[9] Alex S. Szalay,[5] Barry Y. Welsh,[10] and Sukyoung K. Yi[7]

Received 2007 April 24; accepted 2007 July 19

ABSTRACT

Using a sample of galaxies from the Sloan Digital Sky Survey spectroscopic catalog with measured star formation rates (SFRs) and ultraviolet (UV) photometry from the *GALEX* Medium Imaging Survey, we derived empirical linear correlations between the SFR to UV luminosity ratio and the UV–optical colors of blue-sequence galaxies. The relations provide a simple prescription to correct UV data for dust attenuation that best reconciles the SFRs derived from UV and emission-line data. The method breaks down for the red-sequence population as well as for very blue galaxies such as the local "supercompact" UV luminous galaxies and the majority of high-redshift Lyman break galaxies, which form a low-attenuation sequence of their own.

Subject headings: galaxies: evolution — galaxies: fundamental parameters — surveys — ultraviolet: galaxies

1. INTRODUCTION

Although directly tracing young massive stars, the ultraviolet (UV; $\lambda \sim 912$–3000 Å) luminosity of a galaxy is not a straightforward measure of its current star formation rate (SFR); nor, in fact, is any other observable related to newborn stars. In particular, the galaxy's dust content and past star formation history (SFH) have a significant influence on the interpretation of the observed UV flux in terms of current star production. A large, sometimes dominant fraction of the UV emission may be obscured by dust and reprocessed at far-infrared (FIR) wavelengths. The UV spectral slope is commonly used to estimate this fraction (Meurer et al. 1999), but it is strongly affected by the SFH (Kong et al. 2004). Also because UV-emitting stars live long enough for successive generations to coexist, the SFH over the past few hundred Myr must be known to translate the dust-corrected UV flux into a more instantaneous SFR, such as derived from the galaxy's Hα emission. In the case of a constant SFR and in the absence of dust, the UV luminosity to SFR ratio reaches a plateau after $\sim 10^8$ yr (e.g., Kennicutt 1998), but a strong starburst will cause the UV luminosity to scale differently with the SFR. Interpreting the UV emission of early-type galaxies is also less straightforward due to contamination by older stars (Ree et al. 2007).

Dust obscuration and SFH may be estimated with the help of additional data (e.g., the Balmer decrement or far-infrared emission for the dust, the Balmer break for the SFH) and of theoretical assumptions. However, such additional information is not always available or in fact acquirable, in particular at high redshifts, where SFRs are generally derived from UV and/or infrared (IR) photometry with rather large uncertainties. New near-IR spectrographs on 8–10 m telescopes are now making it possible to detect Hα emission and/or continuum breaks at $z > 2$ (van Dokkum et al. 2005; Erb et al. 2006b; Kriek et al. 2006a, 2006b), but the technique is still limited to prominent features. Detecting Hα at $z \sim 2$ implies a SFR greater than a few $M_\odot$ yr^{-1} (Erb et al. 2006b), which is not representative of the whole population (Kriek et al. 2006b). Optical images that pick up the rest-frame UV at $z > 2$ remain the easiest data to obtain.

Here we use medium deep UV photometry from the *Galaxy Evolution Explorer* (*GALEX*) and the wealth of additional data provided by the Sloan Digital Sky Survey (SDSS) to derive simple empirical relations between the observed UV luminosity and the SFR of local star-forming galaxies. SFRs were derived for tens of thousands of SDSS galaxies using their emission lines and state-of-the-art models including a consistent treatment of the dust from the UV to the far-IR (Brinchmann et al. 2004). We assume these SFRs to be the best possible estimates at the present time, given the quality of the spectrophotometric data and the tested reliability of the models, and present an empirical method to recover them from the UV luminosity of galaxies using their UV–optical colors. We compare our relations with existing methods, in particular attenuation estimates based on the slope of the UV continuum, which are commonly used, and investigate their limitations both locally and at high redshift.

The data are summarized in § 2. In § 3 we review the relation between the UV luminosity and the SFR of star-forming galaxies, as well as several published methods for estimating their UV attenuation. In § 4 we present simple empirical color relations that best reconcile the UV data with the SFR estimates based on

[1] Laboratoire d'Astrophysique de Marseille, BP 8, Traverse du Siphon, 13376 Marseille Cedex 12, France.
[2] California Institute of Technology, MC 405-47, 1200 East California Boulevard, Pasadena, CA 91125; treyer@srl.caltech.edu.
[3] Department of Astronomy, Columbia University, MC 2457, 550 West 120 Street, NY, NY 10027.
[4] Observatories of the Carnegie Institution of Washington, 813 Santa Barbara Street, Pasadena, CA 91101.
[5] Laboratory for Astronomy and Solar Physics, NASA Goddard Space Flight Center, Greenbelt, MD 20771.
[6] Center for Astrophysical Sciences, The Johns Hopkins University, 3400 North Charles Street, Baltimore, MD 21218.
[7] Department of Physics and Astronomy, The Johns Hopkins University, Homewood Campus, Baltimore, MD 21218.
[8] Center for Space Astrophysics, Yonsei University, Seoul 120-749, South Korea.
[9] Department of Physics and Astronomy, University of California, Los Angeles, CA 90095.
[10] Space Sciences Laboratory, University of California at Berkeley, 601 Campbell Hall, Berkeley, CA 94720.

emission-line measurements and discuss their limitations. Our conclusions are presented in § 5. Throughout the paper we assumed a flat ΛCDM cosmology with $H_0 = 70$ km s^{-1} Mpc^{-1}, $\Omega_M = 0.3$ and $\Omega_\Lambda = 0.7$, and a Kroupa IMF (Kroupa 2001).

2. DATA AND DERIVED PHYSICAL QUANTITIES

We select galaxies from the SDSS spectroscopic catalog (Data Release 4; Adelman-McCarthy 2006) with near-UV (NUV) and far-UV (FUV) photometry from the *GALEX* Medium Imaging Survey (Internal Release 1.1; Martin et al. 2005; Morrissey et al. 2005, 2007). The UV filters have effective wavelengths of 1528 and 2271 Å, respectively. The Medium Imaging Survey (MIS) has a 5 σ detection limit of 22.7 (AB magnitude) in both filters for a typical exposure. This magnitude limit corresponds to a cut in magnitude error of ∼0.1 in the NUV band and ∼0.2 in the FUV band (Bianchi et al. 2006, their Fig. 2). Our primary sample consists of 23,400 SDSS galaxies with $r < 17.8$, $z > 0.005$, measured Hα emission, aperture corrections less than 1.3 dex (defined as the ratio of the total SFR to the SFR estimated within the fiber; see below), and *GALEX* coverage in the NUV band. Adding FUV coverage reduces the sample to 17,500 galaxies due to occasional failures of the *GALEX* FUV detector. Galaxies flagged as active galactic nuclei (AGNs) in the SDSS MPA/JHU DR4 value-added catalogs have been excluded.

The physical properties of SDSS galaxies were analyzed in detail by Kauffmann et al. (2003a, 2003b); Tremonti et al. (2004), and Brinchmann et al. (2004, hereafter B04) among others. In particular, the full likelihood distributions of their SFRs were derived by fitting all strong emission lines simultaneously using the Charlot & Longhetti (2001) models, following the methodology of Charlot et al. (2002) (B04). Dust is accounted for with the Charlot & Fall (2000) multicomponent model, which provides a consistent treatment of the attenuation of both continuum and emission-line photons. The dust attenuation is based on the Hα/Hβ ratio to first order but is really constrained by all the lines. B04 also devised a method for estimating the SFR of early-type galaxies with no detectable Hα emission from their 4000 Å break index, but we excluded those from our sample. We use the medians of the SFR distributions and consider these values, noted SFR$_e$ (for emission lines, following B04), to be the best currently available estimates of the SFR given the quality of the data and the technique used to derived them. Uncertainties are discussed in detail in the original paper.

Other quantities such as 4000 Å break indices and stellar masses (Kauffmann et al. 2003a) are also available from the SDSS MPA/JHU DR4 value added catalogs.[11] The stellar mass is defined as the total mass of stars formed over the lifetime of the galaxy. The 4000 Å break index—$D_n(4000)$—is defined as the ratio of the average flux density F_ν in the narrow bands 3850–3950 and 4000–4100 Å following Balogh et al. (1998). It is a relatively dust-insensitive measure of a galaxy's SFH, equivalent to the ratio of the SFR averaged over the last $\sim 10^{8.5}$ yr to the SFR averaged over $>10^9$ yr (Johnson et al. 2007). The $D_n(4000)$ distribution is strongly bimodal around $D_n(4000) \sim 1.6$, dividing galaxies into the well-known "red sequence" of early-type, old-star–dominated galaxies [$D_n(4000) \gtrsim 1.6$] and the "blue cloud" of late-type galaxies with recent star formation [$D_n(4000) \lesssim 1.6$; Kauffmann et al. 2003a; Strateva et al. 2001]. In the following we refer to these two populations as simply red and blue galaxies.

Our final two samples consist of the 20,800 galaxies in the primary sample (89%) that have been detected by *GALEX* in the NUV band (SDSS+NUV sample), and of the 14,900 galaxies in the primary sample with additional FUV coverage (85%) that have been detected both in the NUV and FUV bands (SDSS+NUV+FUV sample). In the following we use the larger, SDSS+NUV-only sample whenever FUV fluxes are not explicitly needed. These samples are strongly biased against red-sequence galaxies but complete for blue galaxies: ∼98% of $D_n(4000) < 1.6$ galaxies are detected in the NUV band (and in the FUV band when both are available) against ∼72% of $D_n(4000) > 1.6$ galaxies (∼52% in both UV bands when both are available). The average magnitude error is 0.03 in the NUV band and 0.07 in the FUV band for the blue population, 0.08 in the NUV band and 0.16 in the FUV band for the red population.

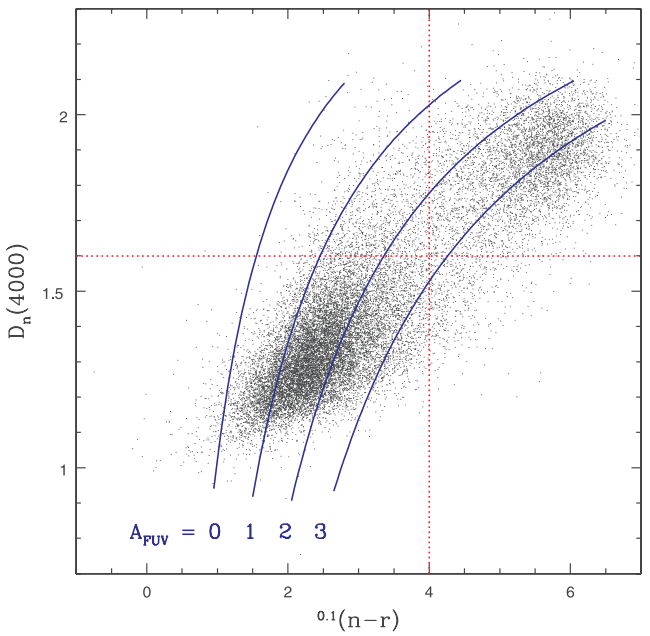

FIG. 1.— The 4000 Å break index, $D_n(4000)$, as a function of $^{0.1}(n - r)$ for the SDSS+NUV sample. The blue curves represent lines of equal FUV attenuation by Johnson et al. (2007). The horizontal and vertical dotted lines at $D_n(4000) = 1.6$ and $^{0.1}(n - r) = 4$ mark the boundaries between the "red sequence" and "blue cloud" populations.

We derive absolute magnitudes in all the bands from the redshift and the Galactic extinction-corrected SDSS+*GALEX* photometry using the `kcorrect v4_1` software of Blanton & Roweis (2007). In order to minimize the uncertainties on the *k*-corrections, the magnitudes are *k*-corrected to the mean redshift of the SDSS sample ($\bar{z} = 0.1$) and are noted $^{0.1}$mag, where mag = *f* or *n* for the *GALEX* FUV and NUV bands, and *g*, *r*, *i*, and *z* for the SDSS bands. The *k*-correction at redshift $\bar{z}$ is by definition $-2.5 \log (1 + \bar{z})$ in all bands for all galaxies and deviates from this value toward both ends of the redshift range ($0.005 < z < 0.28$). In the UV bands, this deviation is less than 0.1 mag for 95% of the galaxies.

Figure 1 shows the distribution of the SDSS+NUV sample in the $^{0.1}(n - r)$ versus $D_n(4000)$ plane. The $^{0.1}(n - r)$ color distribution is strongly bimodal (Wyder et al. 2007) with $^{0.1}(n - r) = 4$ defining roughly the same boundaries as $D_n(4000) = 1.6$ between the red and blue populations. Galaxies with $^{0.1}(n - r) < 4$ and $D_n(4000) < 1.6$ (the "blue cloud") represent 70% of the sample (81% of the SDSS+NUV+FUV sample); galaxies with $^{0.1}(n - r) > 4$ and $D_n(4000) > 1.6$ (the "red sequence") represent 22% of the sample (10% of the SDSS+NUV+FUV sample). The solid lines are polynomial fits to the dust/color/SFH relation derived by Johnson et al. (2007; see § 3) for given values of the FUV attenuation as marked in the figure. The fits are

[11] See http://www.mpa-garching.mpg.de/SDSS.

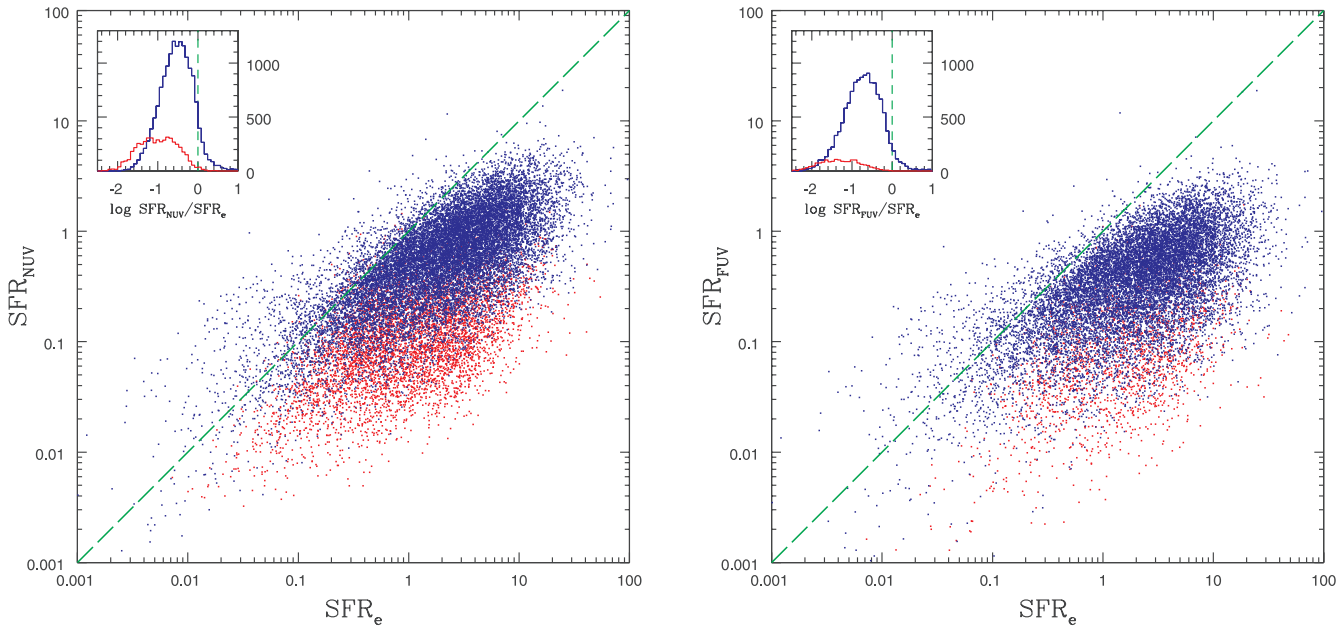

FIG. 2.—Uncorrected UV SFRs (SFR_{NUV} on the left, SFR_{FUV} on the right) against the emission-line-derived SFR_e (Brinchmann et al. 2004) in units of $M_\odot$ yr^{-1}. The dashed green lines shows SFR equality. The blue and red dots represent blue- and red-sequence galaxies, defined as $^{0.1}(n-r) < 4$ and $^{0.1}(n-r) > 4$, respectively. The blue and red histograms in each panel are the log (SFR_{UV}/SFR_e) distributions for the two populations. As expected from uncorrected luminosities SFR_{UV} underestimates SFR_e, especially so at high SFR.

good for galaxies with $D_n(4000) < 1.6$ but less reliable for red-sequence galaxies (see Johnson et al. 2007 for details). The model illustrates how broadband colors depend on both the SFH and the amount of dust attenuation.

3. DERIVING A STAR FORMATION RATE FROM AN ULTRAVIOLET FLUX

3.1. *Calibration*

The SFR measured from the UV emission is usually written as

$$\mathrm{SFR}_{\mathrm{UV}}\left(M_\odot\ \mathrm{yr}^{-1}\right) = \frac{L_{\mathrm{UV}}\left(\mathrm{ergs\ s^{-1}\ Hz^{-1}}\right)}{\eta_{\mathrm{UV}}}, \qquad (1)$$

where η_{UV} converges to η^0_{UV} for a constant SFR. Scaled to a Kroupa initial mass function (IMF), the most commonly used factor is $\log(\eta^0_{\mathrm{UV}}) = 28.02$ (Kennicutt 1998). It assumes that the UV spectrum is nearly flat in L_ν over the wavelength range 1500–2800 Å. Using the Bruzual & Charlot (2003) stellar population synthesis models with similar assumptions (solar metallicity, a constant SFH, and a Kroupa IMF), S. Salim (2007, private communication) derived slightly higher factors for the *GALEX* filters: $\log(\eta^0_{\mathrm{FUV}}) = 28.09$ and 28.08. They are little sensitive to metallicity and to the SFH provided the SFR has been nearly constant in the last 10^8 yr. Very young starburst galaxies would significantly deviate from a constant SFR model and require a higher value of η_{UV}, while the UV emission of early-type galaxies is contaminated by older stars. For an optically selected sample with a mix of SFHs and metallicities similar to the SDSS+*GALEX* sample defined in § 2 (the average metallicity of which is 0.8 $Z_\odot$), Salim et al. (2007) suggest using their median conversion factor, $\log(\overline{\eta}_{\mathrm{FUV}}) = 28.14$. We assume this calibration for both UV bands in the following.

Figure 2 shows SFR_{UV} against SFR_e for the NUV and FUV bands (*left and right panels, respectively*), assuming no dust correction for the UV luminosities. The dashed green line denotes equality of SFR. Blue and red dots distinguish between blue and red galaxies defined as having $^{0.1}(n-r) < 4$ and >4, respectively. The histograms in the inset show the distribution of the SFR_{UV}/SFR_e ratios for the blue and red populations. As expected from uncorrected luminosities, SFR_{UV} underestimates the "true" SFR, including for the red population, although part of their UV luminosity is unrelated to the current SFR. The scatter is large in both bands, indicating a large range of UV attenuations for a given SFR or a given UV luminosity. There is also a clear trend with SFR_e in the sense that galaxies with higher SFR tend to require a larger dust correction, as was first observed by Wang & Heckman (1996).

3.2. *Dust Attenuation Estimates*

The fraction of UV flux emitted by newborn stars and absorbed by dust in the galaxy is reradiated at infrared (IR) wavelengths (Buat 1992). Assuming a standard extinction law and that the dust is heated by intrinsically young stellar populations, the FUV attenuation can be approximated by

$$A_{\mathrm{FUV}} = 2.5 \log(\mu \mathrm{IRX} + 1), \qquad (2)$$

where IRX is the ratio of the IR to UV luminosities (the so-called infrared excess) and μ corrects for the fraction of IR luminosity heated by older stars and by light bluer than the FUV band (Meurer et al. 1999). Other relations were derived that yield very similar results (e.g., Buat et al. 2005). UV reddening as measured by the slope β of the UV continuum ($f_\lambda \propto \lambda^\beta$) or a UV color correlates with IRX in starburst galaxies, as expected from a foreground screen of dust (Witt et al. 1992; Calzetti et al. 1994). Thus β or UV colors are often used to estimate A_{FUV}. The IRX/β correlation was recently revisited and corrected by several authors for more "normal" star-forming galaxies using *GALEX* data (Seibert et al. 2005; Cortese et al. 2006; Salim et al. 2007; Johnson et al. 2007). Seibert et al. (2005, hereafter Se05) found that the starburst relation systematically overestimates the FUV attenuation of more quiet galaxy types by 0.58 mag, albeit with a large scatter. They

derived the following empirical relation from a diverse sample of ~200 galaxies with UV photometry from *GALEX* and FIR photometry from the *Infrared Astronomical Satellite* (*IRAS*):

$$A_{\rm FUV}^{\rm Se05} = 3.97\,(m_{\rm FUV} - m_{\rm NUV} - 0.1) + 0.14, \quad (3)$$

where $m_{\rm FUV}$ and $m_{\rm NUV}$ are the apparent magnitudes in the FUV and NUV bands, respectively. The 0.1 mag offset corrects for a change in calibration between the *GALEX* photometry used by Se05 (the internal data release IR0.2) and that used in the present paper (IR1.1; M. Seibert et al., in preparation).

Salim et al. (2007, hereafter Sa07) derived a yet shallower relation between the attenuation and the UV color of normal blue galaxies using a different technique and the much larger *GALEX*+SDSS sample we are using here. They obtained the SFR and FUV attenuations, among other physical properties, by fitting the UV and optical photometry to an extensive library of model spectral energy distributions (SEDs) for which dust attenuation was computed from the same Charlot & Fall (2000) model used by B04. While B04 obtained their SFRs and attenuations from optical emission lines (the Hα line and the Balmer decrement to first approximation), Sa07's are essentially constrained by the UV fluxes and the UV colors, respectively. The agreement is generally good between the two approaches, but discrepancies remain, in particular between the attenuations, as we discuss further below. Sa07 derived the following simple prescription from their extensive modeling for galaxies with ${}^{0}(n-r) < 4$ and ${}^{0}(f-n) < 0.9$:

$$A_{\rm FUV}^{\rm Sa07} = 2.99\ {}^{0}(f-n) + 0.27, \quad (4)$$

where the 0 subscript refers to rest-frame colors k-corrected to $z = 0$. The small (<5%) fraction of galaxies with ${}^{0}(n-r) < 4$ and ${}^{0}(f-n) > 0.9$ are assigned a constant attenuation of 2.96.

Longer baseline colors such as UV−optical colors carry mixed but separable information about the SFH and IRX. Using a sample of galaxies with UV through IR photometry from *GALEX*, SDSS, and *Spitzer*, Johnson et al. (2006, 2007 [hereafter J07]) showed that given the SFH of a galaxy [they used $D_n(4000)$], IRX could be more accurately inferred from UV−optical colors than from UV colors. Assuming equation (2) with $\mu = 0.6$, they derived the following relation for galaxies with $D_n(4000) < 1.6$:

$$A_{\rm FUV}^{\rm J07} = 1.21 - 2.04x + 1.45y - 0.98y^2, \quad (5)$$

where $x = D_n(4000) - 1.25$ and $y = {}^{0.1}(n-r) - 2$.

We note as $\rm SFR_{FUV,\,corr}$ the SFR derived from the UV luminosity corrected for dust attenuation using one of the above equations. Figure 3 shows $\rm SFR_{FUV,\,corr}$ against $\rm SFR_{\it e}$ for the blue galaxies [${}^{0.1}(n-r) < 4$] using equations (3) (Se05), (4) (Sa07), and (5) (J07) as indicated. In each panel the dotted, dashed, and solid blue lines show the ordinary least-square (OLS) regression of the Y-axis on the X-axis, the OLS regression of the X-axis on the Y-axis, and the bisector of those two lines, respectively (Isobe et al. 1990). We choose the bisectors as the "best-fit" lines, here and in the rest of the paper. The best-fit slopes, variances, correlation coefficients, and residual scatters are listed in Table 1 for the three attenuation models (first three lines). The histograms show the distributions of the $\rm SFR_{FUV,\,corr}/SFR_{\it e}$ ratios compared to the distribution of the uncorrected $\rm SFR_{FUV}/SFR_{\it e}$ ratios. The averages of the distributions are also listed in Table 1. All three methods provide a very good average correction with a reduced scatter compared to the uncorrected $\rm SFR_{FUV}$, especially so for the J07 correction. However, a residual trend with $\rm SFR_{\it e}$ remains in the sense that galaxies with the highest and lowest SFR tend to be under- and overcorrected, respectively. This indicates that the models do not quite sufficiently scale with the SFR to straighten up the uncorrected correlation in Figure 2. The trend is minimal for the Se05 correction for which the scatter is largest and most pronounced for the J07 correction for which the scatter is otherwise best reduced. This trend with $\rm SFR_{\it e}$ is the same as that noted by Sa07 as a trend with mass (their Fig. 8) and by J07 as a trend with ${}^{0.1}(n-r)$ and $D_n(4000)$ (their Figs. 12 and 13). Indeed mass and to a lesser extent colors and $D_n(4000)$ correlate with $\rm SFR_{\it e}$. The reason for it remains unclear, but Sa07 concluded that the most likely interpretation in the framework of their modeling was that attenuations were less well constrained by the UV data than by the emission lines at the two ends of the distribution. In the case of J07, the parametric relation between IRX, $D_n(4000)$ and ${}^{0.1}(n-r)$ is a good fit to blue galaxies, more so than between IRX and UV color (see J07 for a detailed discussion). Therefore it is perhaps the relation between IRX and $A_{\rm FUV}$ that is not totally adequate. We return to this point in the next section.

4. RECONCILING UV AND EMISSION-LINE STAR FORMATION RATES

4.1. *Empirical Color Corrections*

Assuming as we do that $\rm SFR_{\it e}$ is the current best dust-corrected SFR estimate and that our choice of $\eta_{\rm UV}$ is adequate, the UV attenuation (FUV or NUV) can be directly measured as

$$A_{\rm UV} = -2.5\log(\rm SFR_{UV}/SFR_{\it e}). \quad (6)$$

We now revisit the color dependence of these known attenuations. Figure 4 (*left panel*) shows the $\rm SFR_{NUV}/SFR_{\it e}$ ratios as a function of ${}^{0.1}(n-r)$ for the SDSS+NUV sample. The solid lines show the OLS bisector for each bin as shown in inset. The three bins making up the blue sequence [$D_n(4000) < 1.6$] add up to form a single tight correlation, while the two bins with $D_n(4000) > 1.6$ form a scattered cloud. For galaxies with $D_n(4000) < 1.6$ and ${}^{0.1}(n-r) < 4$, the bisector fit is

$$A_{{\rm NUV},\,n-r} = 1.71\ {}^{0.1}(n-r) - 2.86, \quad (7)$$

with a linear correlation coefficient $r = 0.77$ and rms = 0.70. The SDSS+NUV sample allows us to see the impact of the SFH on the attenuation/color relation. It is bimodal to first order: attenuation is linearly dependent on color for blue-sequence galaxies and practically independent of it for red-sequence galaxies. Similar correlations are found when using FUV luminosities and/or other UV−optical colors. Using the FUV luminosity and ${}^{0.1}(f-g)$ yields

$$A_{{\rm FUV},\,f-g} = 1.84\ {}^{0.1}(f-g) - 2.57. \quad (8)$$

The correlation is tighter than equation (7) ($r = 0.84$, rms = 0.66). On the other hand, ${}^{0.1}(f-n)$ results in a poorer and more scattered correlation ($r = 0.56$, rms = 1.02):

$$A_{{\rm FUV},\,f-n} = 4.05\ {}^{0.1}(f-n) - 0.18. \quad (9)$$

The last two correlations are shown in the right panel of Figure 4. The latter correlation is similar to that proposed by Cortese et al. (2006, their Fig. 10) using $\log(L_{\rm H\alpha}/L_{\rm FUV})$ as a function of $(m_{\rm FUV} - m_{\rm NUV})$ for a small sample of star-forming galaxies in the Coma Cluster. It is consistent with equation (3) (Se05) but a much steeper function of UV color than equation (4) (Sa07).

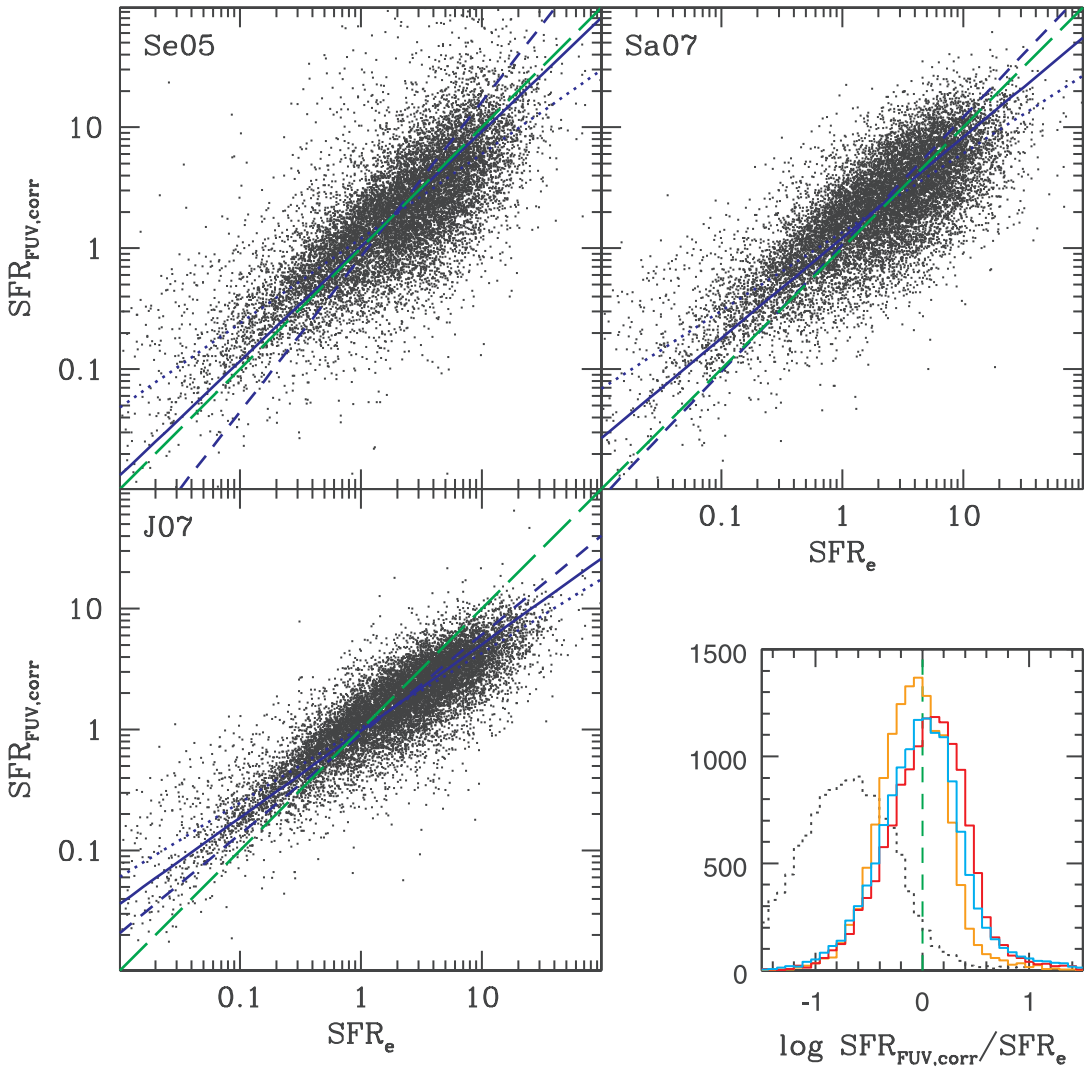

FIG. 3.—Dust-corrected FUV SFRs ($SFR_{FUV,\,corr}$) against SFR_e for the blue population [$^{0.1}(n-r) < 4$] using the FUV attenuation methods of Se05, Sa07, and J07 as indicated. The SFRs are in units of $M_\odot\ yr^{-1}$. The dotted, dashed, and solid blue lines in each panel are the ordinary least-square (OLS) regression of the *Y*-axis on the *X*-axis, the OLS regression of the *X*-axis on the *Y*-axis and the bisector of those two lines, respectively. The histograms show the distributions of the $SFR_{FUV,\,corr}/SFR_e$ logarithmic ratios: light blue, red, and orange for Se05, Sa07, and J07, respectively. The dotted histogram is the distribution of the uncorrected SFR_{FUV}/SFR_e ratios. All three models provide a very good average correction but tend to over (under) correct galaxies with the lowest (highest) SFRs.

However, all three equations, as well as equation (8), converge for the majority of galaxies around the peak of the color distribution [$^{0.1}(n-r) \sim 2.4-2.5$] and yield similar average values in good agreement with the measured average attenuation ($\langle A_{FUV}\rangle \sim 1.8$). Equation (5) (J07) yields a slightly lower average attenuation of 1.6. Discrepancies between these corrections are largest for the reddest and bluest galaxies.

We note as $SFR_{FUV,c}$ the FUV-based SFRs corrected using one of the functions of color derived in this section. Figure 5 shows $SFR_{FUV,c}$ against SFR_e using $A_{FUV,f-n}$ (*left panel*) and $A_{FUV,f-g}$ (*right panel*) for the blue population. The correlation is very close to equality in both cases, as expected since the corrections were designed to minimize $SFR_{FUV,c}/SFR_e$, and the scatter is best reduced using $^{0.1}(f-g)$, as expected as well from the

TABLE 1
CORRELATION PARAMETERS BETWEEN THE CORRECTED FUV SFR ($SFR_{FUV,\,model}$) AND SFR_e

Model	Slope *a*	Var(*a*)	*r*	rms	$\langle SFR_{FUV,\,model}/SFR_e\rangle$
Se05	0.9498	5.181e-05	0.7392	0.4209	0.0012
Sa07	0.8314	2.23e-05	0.7866	0.3328	0.0421
J07	0.7171	1.242e-05	0.8658	0.2278	−0.0847
Equation (9)	0.9799	5.14e-05	0.7487	0.4266	0.0061
Equation (8)	0.9258	1.915e-05	0.8705	0.2893	0.0316

NOTES.—Correlation parameters are for the various attenuation models described in the text as listed in the first column. The next columns list the slope *a* of the linear correlation fitted to the $SFR_{FUV,\,model}$ vs. SFR_e relation, the variance of the slope, the correlation coefficient, the rms, and the average of the $SFR_{FUV,\,model}/SFR_e$ ratios.

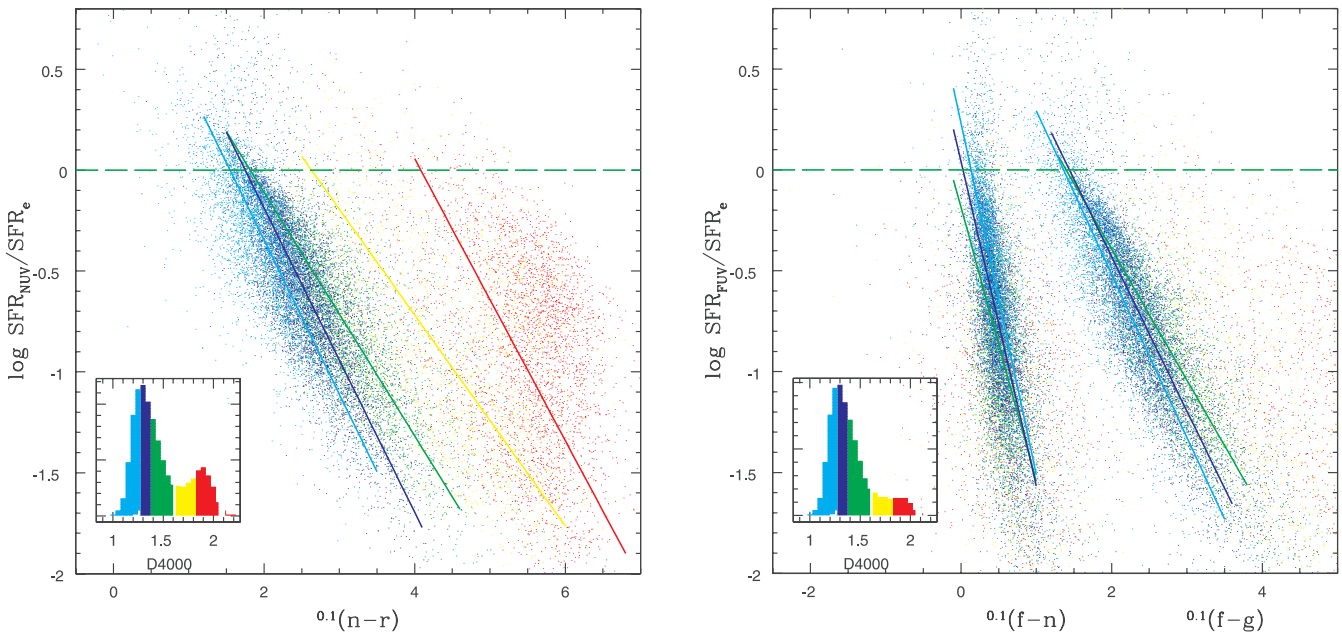

FIG. 4.—Color dependence of the SFR_{UV}/SFR_e ratio for different bins of $D_n(4000)$. *Left:* $\log(SFR_{NUV}/SFR_e)$ against $^{0.1}(n-r)$ for the SDSS+NUV sample; *right:* $\log(SFR_{FUV}/SFR_e)$ against $^{0.1}(f-g)$ and against $^{0.1}(f-n)$ for the SDSS+NUV+FUV sample. The data are color-coded to match the binned $D_n(4000)$ distribution histogram shown in inset. The colored solid lines show the fitted linear correlations in each bin of $D_n(4000)$. The three bins making up the "blue cloud" population [$D_n(4000) < 1.6$; *light blue*, *dark blue*, *and green* are tightly correlated with color, while the two bins forming the red sequence $D_n(4000) > 1.6$; *yellow and red*] are practically independent of it. The color correlations observed for blue galaxies provide simple UV attenuation corrections (see text for details).

higher correlation coefficient in equation (8). However, a small residual trend with SFR_e remains in this case, which means that the SFR dependence of the attenuation is not completely accounted for by the color dependence [$\log(SFR_{UV}/SFR_e)$ would be better fitted by a linear function of color plus a linear function of $\log(SFR_e)$]. The trend practically disappears when using $^{0.1}(f-n)$, but the correlation is less significant, as in the case of Se05. The parameters of the fits are listed in Table 1 for comparison with the corrections presented in § 3.2. There is a small trade-off between the scatter and the trend with SFR_e (the lower the rms, the more the slope deviates from unity) except for the empirical $^{0.1}(f-g)$ correction for which the combination of trend and scatter is best reduced ($a > 0.9$ and rms < 0.3). Figure 6 shows the difference between the measured attenuation (eq. [6]) and the four parametric estimates (Se05, Sa07, J07, and eq. [8]) as a function of SFR_e ($\Delta A_{FUV} = A_{FUV} - A_{FUV,\,model}$). The red curves are isodensity contours. The dashed green lines mark $\Delta A_{FUV} = -1$, 0, and 1. All four methods converge with A_{FUV}

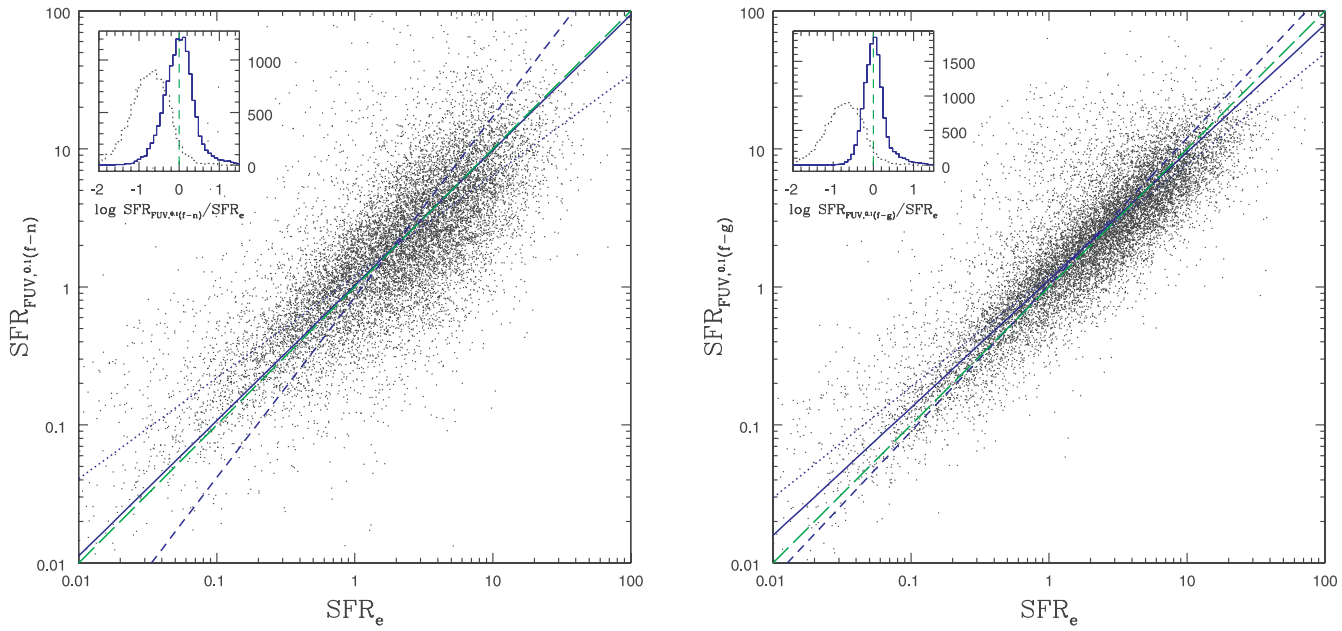

FIG. 5.—Color-corrected FUV SFRs against SFR_e. The FUV luminosities are corrected using the correlations established in Fig. 4 between A_{FUV} and $^{0.1}(f-n)$ (eq. [9]; *left panel*) and between A_{FUV} and $^{0.1}(f-g)$ (eq. [8]; *right panel*). The histograms in inset show the distributions of $\log(SFR_{FUV}/SFR_e)$ with and without corrections (*solid and dotted lines, respectively*). SFR_e is best recovered using the $A_{FUV}/^{0.1}(f-g)$ correlation.

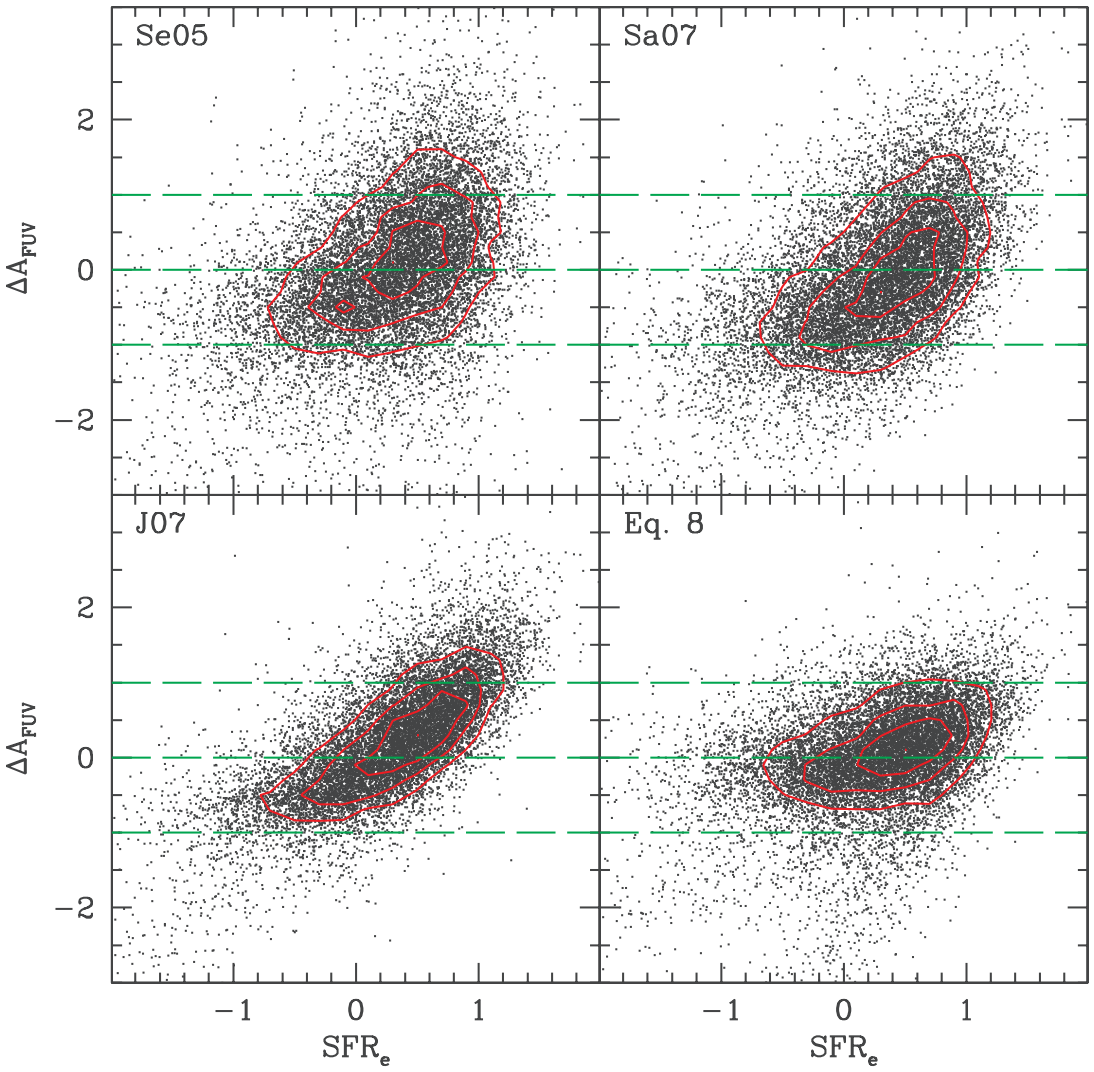

FIG. 6.—$\Delta A_{FUV} = A_{FUV} - A_{FUV,\,model}$ as a function of SFR$_e$ for the various models described in the text as indicated (Se05, Sa07, J07, and eq.[8]). The dashed lines mark $\Delta A_{FUV} = -1$, 0, and +1. The red curves are isodensity contours. All four methods converge with A_{FUV} around the peak of the SFR distribution ($\sim 2\ M_\odot\ \mathrm{yr}^{-1}$) and provide good average corrections, but eq. (8) [the $A_{FUV}{}^{0.1}(f-g)$ correlation] minimizes ΔA_{FUV} and its dependence with SFR$_e$ for the majority of the galaxies.

around the peak of the SFR distribution ($\sim 2\ M_\odot\ \mathrm{yr}^{-1}$), and as noted above, provide good average corrections, but equation (8) minimizes ΔA_{FUV} for the majority of the galaxies, as well as the dependence with SFR$_e$. Although the improvement is by no means dramatic, it provides an estimate of the FUV attenuation that best recovers the SFR derived from emission lines at an equivalent or lower "cost," since at least one optical photometric measurement and the redshift are required for *k*-corrections in all cases.

4.2. *Discussion*

As aperture corrections are an important source of uncertainty in deriving total SFRs from the SDSS fiber spectra, we check that the above correlations are not affected by aperture effects. We define the aperture correction (AC) as the ratio of the total SFR (SFR$_e$) to the SFR estimated within the fiber (B04) and split the blue sample into three bins of increasing aperture correction. Figure 7 shows the SFR$_{FUV}$/SFR$_e$ ratios as a function of $^{0.1}(f-g)$ for the three bins (*inset*), shifted by a constant as indicated for clarity. The solid lines show the bisector fits in each bin, and the dashed lines show equation (8) shifted by the appropriate amount for comparison. No significant difference is seen in the correlation itself as a function of aperture correction, but galaxies with SFR$_{FUV}$ > SFR$_e$ (yielding a negative FUV attenuation) have systematically high aperture corrections (and low redshift). It is likely that in these large nearby galaxies, the fiber missed off-centered regions of enhanced star formation and that SFR$_e$ was underestimated.

Another source of uncertainty may lie in the definition of the UV attenuation (eq. [6]). Allowing η_{UV} to vary, the SFR$_{UV}$/SFR$_e$ ratio would no longer be a measure of attenuation alone, but a combination of A_{FUV} and η_{UV}: $\log(\mathrm{SFR}_{UV}/\mathrm{SFR}_e) = -0.4A_{UV} + \log(\eta_{UV}/\overline{\eta}_{UV})$. B04 showed that the conversion factor $\eta_{H\alpha}$ from Hα luminosity to SFR ($\eta_{H\alpha} = L_{H\alpha}/\mathrm{SFR}_e$) decreases with mass (and metallicity), spanning nearly 0.4 dex in the range of mass (and metallicity) spanned by the SDSS sample. This is interpreted as massive metal-rich galaxies producing less Hα than low-mass, metal-poor galaxies for the same SFR. However, η_{UV} is much less sensitive to metallicity than Hα; consequently, SFR$_{UV}$/SFR$_e$ is expected to be a nearly direct measure of UV attenuation except perhaps for galaxies with very low UV attenuation and metallicity. In any case, the $\sim$1 dex variation in η_{UV} required to straighten up the trend seen in Figure 6, most notably for the J07 dust correction, is definitely ruled out. Let us note that

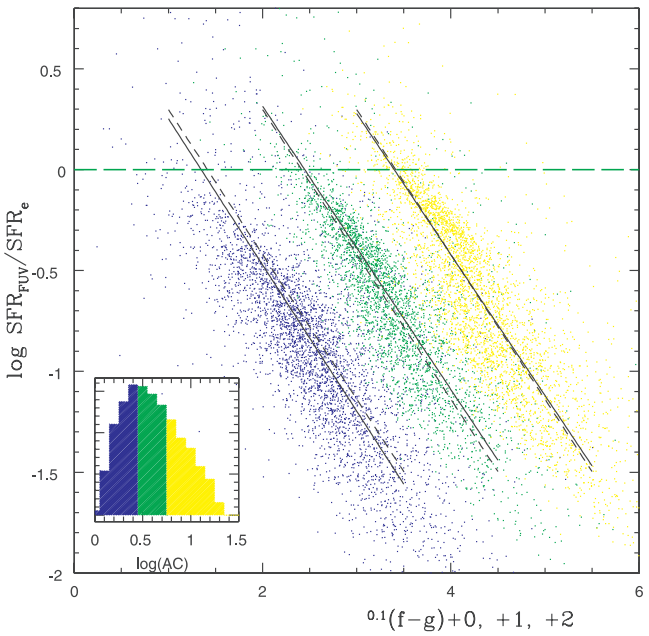

FIG. 7.—SFR$_{FUV}$/SFR$_e$ ratio as a function of $^{0.1}(f-g)$ in three bins of aperture corrections (AC) as shown in inset. The AC is defined as the ratio of the total SFR (SFR$_e$) to the SFR within the SDSS fiber. For clarity the data are shifted by 0, +1, and +2 for the first, second, and third bin, respectively. The solid lines are the linear fits in each bin, while the dashed lines show the correlation for the full sample (eq. [8]) shifted by the appropriate amount. Aperture effects do not bias the correlation.

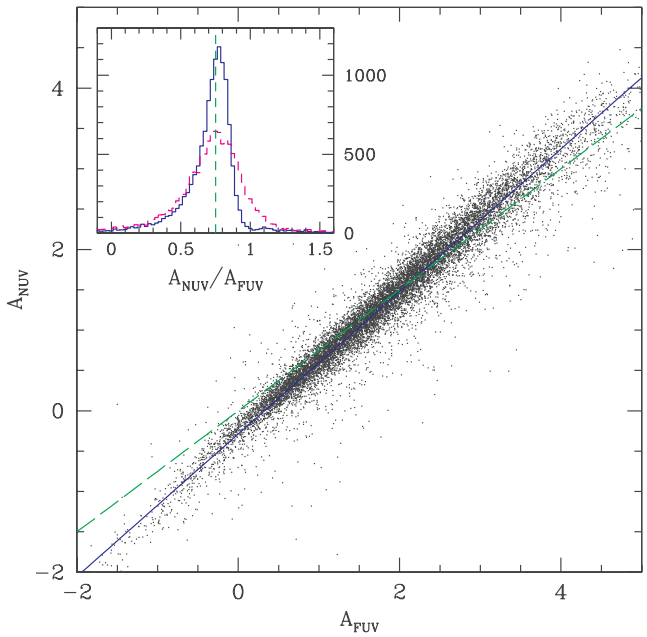

FIG. 8.—Relation between A_{NUV} and A_{FUV} as defined by the SFR$_{UV}$/SFR$_e$ ratios (eq. [6]). The solid blue line is the fitted correlation; the dashed green line at $A_{NUV} = 0.75A_{FUV}$ is the ratio expected from a $\lambda^{-0.7}$ absorption curve (Charlot & Fall 2000). The distribution of the A_{NUV}/A_{FUV} ratios is shown in inset (*solid histogram*) with that of the fits ratios ($A_{NUV,n-r}/A_{FUV,f-g}$; *dotted histogram*). The median ratio for the measured quantities is 0.74 (0.75 for the fits), in excellent agreement with the prediction.

equation (8) can be used to recover SFR$_e$ from the observed UV luminosity whatever the interpretation of the SFR$_{UV}$/SFR$_e$ ratio, provided $\overline{\eta}_{UV}$ is assumed in equation (1). Figure 8 shows the relation between A_{NUV} and A_{FUV} as defined in equation (6). The solid blue line is the best linear fit; the dashed green line at $A_{NUV} = 0.75A_{FUV}$ is the ratio expected from a $\lambda^{-0.7}$ absorption curve (Charlot & Fall 2000). The distribution of the A_{NUV}/A_{FUV} ratios is shown in inset as a solid histogram, and that of the $A_{NUV,n-r}/A_{FUV,f-g}$ ratios as a dotted histogram. The median ratio for the measured quantities is 0.74 (0.75 for the fits), in excellent agreement with the prediction. The *GALEX* data are therefore consistent with the attenuated UV fluxes predicted by the dust model used to derive SFR$_e$ from independent emission-line measurements.

As noted in § 3.2, the relation between IRX and A_{FUV} may be responsible for the discrepancy between A_{FUV} and A_{FUV}^{J07} (eq. [5]). Figure 9 shows the relation between A_{FUV} (eq. [6]) and IRX derived from $D_n(4000)$ and $^{0.1}(n-r)$ (eqs. [2] and [5]). The solid line is the relation used by J07 to relate the two quantities (eq. [2] with $\mu = 0.6$). While it is appropriate for the average galaxy, it becomes discrepant at the blue and red ends (or for the least and most massive star-forming galaxies). There is also a large range of attenuations for a given IRX. A color (or SFR) dependent μ parameter accounting for the fraction of IR flux due to newborn stars (as opposed to preexisting older stars) would remedy some of the discrepancy. A blue galaxy would have little dust attenuation, little FIR emission for a given UV flux (a small IRX) and its little FIR emission would seem to have little to do with the newborn stars (small μ). At the other end, a red (star-forming) galaxy would be a dusty galaxy with a high SFR, and its large FIR emission (large IRX) would be entirely due to the heating of dust by its new stars (large μ). A μ parameter as large as 2 (meaning that the obscured UV emission would have to be twice the observed FIR emission) is actually necessary to reach the upper envelope of the IRX/A_{FUV} distribution. This might be accounted for by the uncertainty in the IR flux estimate, or by a large fraction of obscured UV photons being reprocessed at wavelengths other than IR. J07 modeled the contribution of newborn stars to IRX as a function of galaxy color and arrived at the opposite conclusion: red galaxies have a higher contribution of older stars to their IR emission than blue galaxies and should therefore require a lower μ, making the trend between the corrected UV luminosity and SFR$_e$ even more pronounced. The validity of SFR$_e$ at low and high mass may of course be questioned, but it seems that the estimate of the IR flux and the interpretation of IRX in terms of FUV attenuation currently involve more uncertainties than the interpretation of the optical data.

4.3. *Limitations: The Oldest and Youngest Galaxies*

The color corrections do not apply to red-sequence galaxies in the local sample. Dust attenuation estimates based on correlations between IRX and colors do not apply well to early-type galaxies either, both the UV and IR SEDs of such galaxies being much less directly related to the emission of young stars than those of late-type galaxies (J07). This is not a drastic limitation to the various methods since red-sequence galaxies contribute little to the overall SFR in the local universe, and even less as redshift increases. But we would like to know whether the above correlations between attenuation and UV–optical color apply to star-forming galaxies at higher redshift, where rest-frame UV fluxes are generally corrected using the IRX/β correlation of local starburst galaxies (Meurer et al. 1999).

Although no spectroscopic data exist at high redshift that allow the same emission-line fitting technique as the SDSS spectra, we can use the unique sample of Erb et al. (2006b), who were able to acquire Hα flux measurements for 114 UV-selected galaxies at $z \sim 2$, for which optical and NIR photometry is also available.

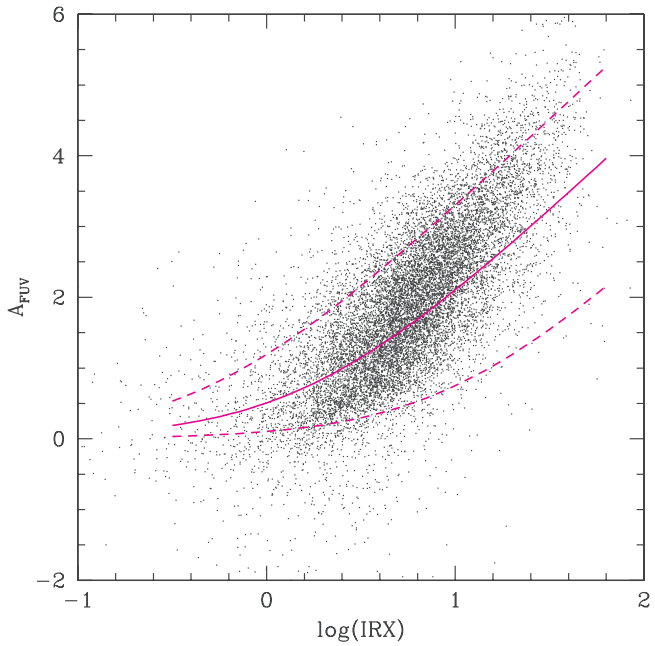

FIG. 9.— FUV attenuation (eq. [6]) as a function of IRX derived from $D_n(4000)$ and $^{0.1}(n-r)$ following Johnson et al. (2007) for the blue population. The solid line is the A_{FUV}/IRX relation of Meurer et al. (1999; eq. [2]) assuming $\mu = 0.6$. The lower and upper dotted lines are for $\mu = 0.1$ and 2, respectively.

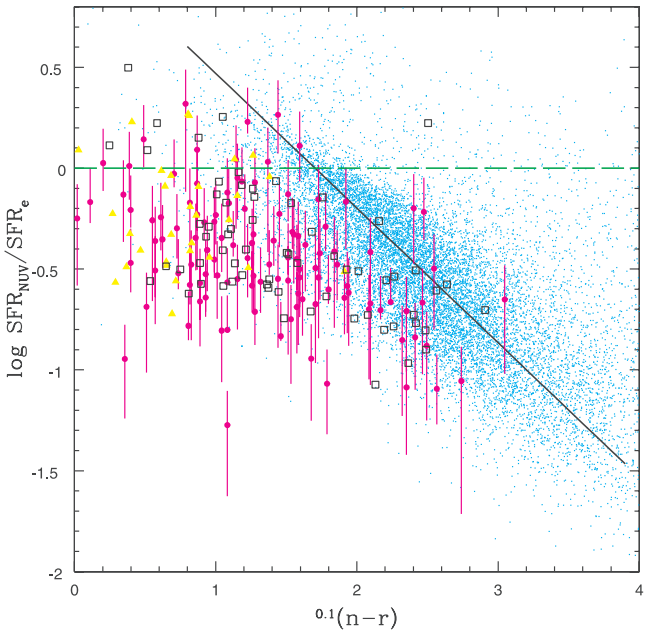

FIG. 10.— SFR_{NUV}/SFR_e ratio as a function of $^{0.1}(n-r)$ for the local blue population (*blue dots*), the sample of local compact and "supercompact" UVLGs of Hoopes et al. (2006; *open squares and filled yellow triangles, respectively*), and the $z \sim 2$ Lyman break galaxy (LBG) sample of Erb et al. (2006b), assuming $SFR_{H\alpha} = SFR_e$ (*pink filled circles*; see text for details). The straight line is the correlation fitted to the local blue population (eq. [7]).

They defined SFR_{FUV} as in equation (1) and $SFR_{H\alpha} = L_{H\alpha}/\eta_{H\alpha}$, using the η_{FUV} and $\eta_{H\alpha}$ values of Kennicutt (1998) converted to a Chabrier (2003) IMF.[12] A factor of 2 aperture correction was also applied to the Hα luminosities. Dust corrections were derived from the best-fit values of $E(B-V)$ obtained from fitting SED models to the multiband photometry and using the extinction law of Calzetti et al. (2000; see Erb et al. 2006b for details). The authors assumed that the color excess of the nebular emission lines was equal to that of the UV continuum, rather than 2.5 times larger as proposed by Calzetti et al. (2000), as it yielded the best agreement between the UV and Hα SFRs after dust correction. The corrected $SFR_{H\alpha}$ are at most 3 times the uncorrected values and less than twice for most of the sample.

As high-redshift galaxies have lower metallicities than local galaxies on average, a higher value of $\eta_{H\alpha}$ might be justified for this sample. However, as both the range of masses and the range of metallicities span by the $z = 2$ galaxies remain within those of the SDSS sample despite evolution in the mass/metallicity relation (Erb et al. 2006a), $\eta_{H\alpha}$ is not expected to be larger than the value predicted for the least massive/most metal-poor galaxies in the local sample, i.e., a factor of 1.5 higher than the Kennicutt value used by Erb et al. (B04, their Fig. 7). We assume the uncorrected values of $SFR_{H\alpha}$ divided by 1.5 to be lower limits to the SFR and use the dust-corrected values as upper limits. We computed the absolute magnitudes of the galaxies in the *GALEX* and SDSS bands from their optical and NIR photometry using `kcorrect v4_1` (Blanton & Roweis 2007).

Figure 10 shows SFR_{NUV}/SFR_e as a function of $^{0.1}(n-r)$, assuming $SFR_{H\alpha} = SFR_e$ for the high-redshift sample and $\eta_{NUV} = \overline{\eta}_{FUV}$ for all galaxies as before. The pink circles are the uncorrected values of $SFR_{H\alpha}$. The upper and lower limits are defined as above. The local blue population is plotted in blue with the correlation derived in § 4.1 (eq. [7]). It is clear that the majority of LBGs that have extremely blue colors do not follow the same correlation as the local galaxies, but the reddest ones [$^{0.1}(n-r) > 1.5$] may still be consistent with the local correlation or show a similar trend with color with only a small blueshift. The bluest LBGs cluster blueward of the local correlation in a region of low UV attenuation.

Also overplotted is a sample of 97 compact UV luminous galaxies (UVLGs) drawn from the present sample and from a cross-match between the SDSS and the larger, shallower *GALEX* All Sky Imaging Survey (Hoopes et al. 2006). SFR_e from B04 are available for all of them. UVLGs (Heckman et al. 2005; Hoopes et al. 2006) are locally rare galaxies defined as having FUV luminosities typical of LBGs: $L_{FUV} > 2 \times 10^{10}\ L_\odot$, corresponding to $\sim 0.3 L_\star$ at $z \sim 3$ (Steidel et al. 1999) but to $\sim 5 L_\star$ at $z \sim 0$ (Wyder et al. 2005). While low surface brightness UVLGs are simply extra large versions of normal spiral galaxies, high surface brightness UVLGs with $I_{FUV} > 10^8\ L_\odot\ \mathrm{kpc}^{-2}$ were found to consist primarily of compact starburst systems. Among these, the "supercompact" UVLGs with $I_{FUV} > 10^9\ L_\odot\ \mathrm{kpc}^{-2}$ bear a remarkable resemblance to high-redshift LBGs for a wide range of physical properties (mass, SFR, metallicity). They are thought to be their closest analogs in the Local universe (Hoopes et al. 2006). Compact and supercompact UVLGs are represented in Figure 10 with open squares and filled triangles, respectively. Both categories occupy the same region of the plot as the high-redshift sample. The supercompact UVLGs are unusually blue [$^{0.1}(n-r) < 1.5$] among the local galaxies, and like the bluest LBGs, lie the furthest away from the bulk of the local population. The extreme blue colors are an indication of strong recent star formation (as well as low attenuation). As noted by Kennicutt (1998), the calibration η_{UV} in equation (1) might be significantly higher for strong starburst galaxies such as these. A higher η_{UV} would lower their SFR_{UV}/SFR_e ratio proportionally and further

[12] To do so, Erb et al. multiplied the Kennicutt factors (computed for a Salpeter IMF) by 1.8; however, a conversion factor of 1.58 between the Salpeter and Chabrier IMFs is more appropriate (S. Salim 2007, private communication). We corrected their SFRs accordingly and multiplied them by 0.94 to account for the small difference between the Chabrier and Kroupa IMFs.

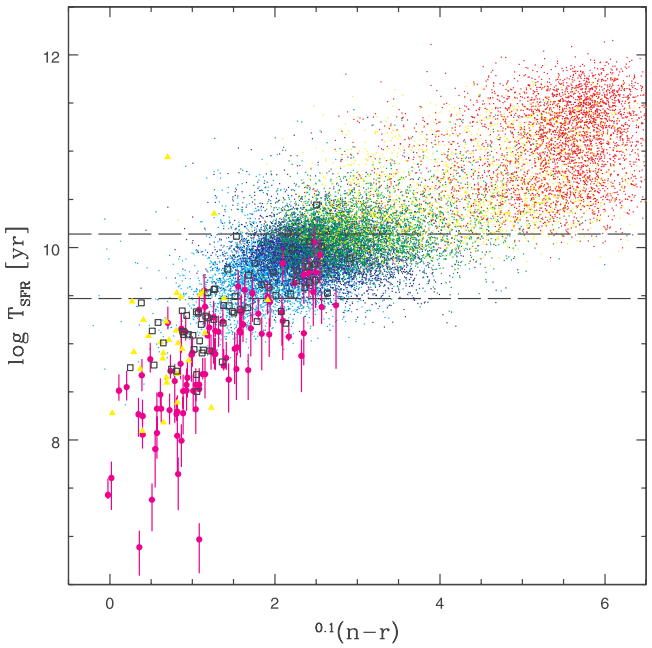

FIG. 11.—SFR timescale $T_{SFR} = M_*/SFR_e$ as a function of $^{0.1}(n-r)$. Local galaxies are shown by dots color coded in bins of $D_n(4000)$ as in Fig. 4. UVLGs and LBGs are represented as in Fig. 10. The two horizontal dashed lines mark the age of the universe at $z = 2$ and $z = 0$ (3 and 13.8 Gyr, respectively). This plot is similar to Fig. 1 with the addition of an ultrablue sequence at $^{0.1}(n-r) < 1.5$ and $T_{SFR} < 3$ Gyr consisting of young compact starburst galaxies for which the local UV attenuation/UV–optical color relations derived in this paper do not apply.

separate them from the main population. Therefore, very blue galaxies with very recent star formation, both locally and at high redshift, form a distinct cluster of their own blueward of the attenuation/color relation of the blue sequence. This locus adds to the blue shift of the attenuation/color relation with $D_n(4000)$ seen in Figure 4 (*left panel*) as those galaxies would have $D_n(4000)$ indices lower than our lowest bin. The reddest of the compact UVLGs and of the LBGs cover a wider range of attenuations that seem to correlate with colors in the same way as local galaxies, only shifted to bluer colors.

$D_n(4000)$ estimates are not available for the high-redshift sample and only available for a fraction of the UVLGs, but we can use the inverse of the specific SFR, $T_{SFR} = M_*/SFR$, as a common SFR timescale for the local and high-redshift samples. Stellar masses were estimated for most of the $z \sim 2$ sample (Erb et al. 2006c). Masses for the *GALEX*+SDSS sample are from Kauffmann et al. (2003a). A third of the UVLGs have mass estimates from this catalog; for the remaining two-thirds we use the values derived by Hoopes et al. (2006) via SED fitting following Salim et al. (2005). The agreement between the mass estimates of Kauffmann et al. (2003a) and Salim et al. (2005) for the *GALEX*+SDDS sample is good, with a rms of 0.12.

As above, we use $SFR = SFR_e$ for the local sample including the UVLGs and $SFR_{H\alpha}$ for the $z \sim 2$ galaxies. Figure 11 shows T_{SFR} as a function of $^{0.1}(n-r)$. The SDSS galaxies are color coded in bins of $D_n(4000)$ as shown in the inset of Figure 4 [this highlights the relation between $D_n(4000)$ and T_{SFR}]. The LBGs are represented by filled circles, the compact UVLGs by open squares, and the supercompact UVGLs by filled triangles. The two horizontal lines correspond to the age of the universe at $z = 0$ and 2 (13.8 Gyr and 3, respectively). Roughly, galaxies with T_{SFR} larger than the age of the universe at their redshift (e.g., nearly all local galaxies with $D_n(4000) > 1.6$ and a few LBGs) have had larger SFR in the past. Inversely, galaxies with T_{SFR} shorter than the age of the universe at their redshift (most LBGs and nearly all the compact UVLGs) must be forming stars more intensely than in the past.

Figure 11 is an analog of Figure 1 with the addition of an "ultrablue" sequence at $^{0.1}(n-r) < 1.5$ and $T_{SFR} < 3$ Gyr consisting of young compact starburst galaxies. The A_{UV}/color correlations derived in § 4.1 hold for galaxies with rather uneventful SFHs (3 Gyr $\lesssim T_{SFR} \lesssim$ 15 Gyr). They are a majority today but may not be when the universe was only ~3 Gyr old, although many LBGs look very much like local blue-sequence galaxies. Furthermore, a dominant fraction of the stellar mass at $z > 2$ is found in redder galaxies which are largely absent from UV surveys (Rudnick et al. 2006; van Dokkum et al. 2006; Marchesini et al. 2007). Kriek et al. (2006b) showed that almost half of their sample of NIR-selected galaxies at $z = 2.0 - 2.7$ have low SFRs and $T_{SFR} > 10$ Gyr (from their Fig. 2). These galaxies are redder than LBGs and would lie in the same part of the plot as the local population.

Although we cannot conclude on the use of the local A_{UV}/color correlation at high redshift, we may expect it to hold for most galaxies to at least intermediate redshifts, or to be slightly shifted to the left as only "mild evolution" of the blue sequence was reported between $z = 0$ and 1 (no change in the number density and colors only ~0.3 mag bluer; Blanton 2006). The luminosity density from UVLGs was found to undergo dramatic evolution between $z = 0$ and 1, reaching >25% of the total FUV luminosity density at $z = 1$ (Schiminovich et al. 2005), but this includes all UVLGs, i.e., mostly very large but otherwise ordinary spiral galaxies. Compact and supercompact UVLGs are very rare in the local universe. Although their evolution with redshift is yet unknown, they are unlikely to dominate the galaxy population at $z = 1$.

5. CONCLUSIONS

Using a large sample of galaxies from the Sloan Digital Sky Survey spectroscopic catalog with measured SFRs and UV photometry from the *GALEX* Medium Imaging Survey, we derived empirical linear correlations between the UV attenuation measured by the SFR to observed UV luminosity ratio, and the UV−optical colors of blue-sequence galaxies [$^{0.1}(n-r) < 4$]. The SFRs were derived from a detailed modeling of the emission lines in the optical spectra (B04) and were considered best estimates. The attenuation/color relation provides a simple prescription to correct UV measurements for dust attenuation in the absence of SDSS quality data. We found or confirmed that other UV attenuation estimates (Se05; Sa07; J07) tend to over (under) correct the UV luminosity of galaxies with the lowest (highest) emission-line SFRs or mass. Using a sample of LBGs (Erb et al. 2006b) at $z \sim 2$ with measured Hα emission, as well as a sample of local compact UV luminous galaxies with LBG-like properties (Hoopes et al. 2006), we found that extremely blue galaxies at both low and high redshift escaped the attenuation/color relation of the blue sequence to form a low-attenuation sequence of their own. As such galaxies are very rare locally and the blue sequence does not evolve much from $z = 0$ to 1 (Blanton 2006; Willmer et al. 2006), we expect our attenuation correction to remain adequate for the majority of galaxies to at least intermediate redshifts.

The authors thank their anonymous referee, whose many comments greatly improved this paper. *GALEX* is a NASA Small Explorer, launched in 2003 April. We gratefully acknowledge NASA's support for its construction, operation, and science analysis, as well as the cooperation of the French Centre National d'Etudes Spatiales and the Korean Ministry of Science and Technology.

REFERENCES

Adelman-McCarthy, J. K., et al 2006, ApJS, 162, 38
Balogh, M. L., Schade, D., Morris, S. L., Yee, H. K. C., Carlberg, R. G., & Ellingson, E. 1998, ApJ, 504, L75
Bianchi, L., et al. 2007, ApJS, 173, 659
Blanton, M. R. 2006, ApJ, 648, 268
Blanton, M. R., & Roweis, S. 2007, AJ, 133, 734
Brinchmann, J., Charlot, S., White, S. D. M., Tremonti, C., Kauffmann, G., Heckman, T., & Brinkmann, J. 2004, MNRAS, 351, 1151 (B04)
Bruzual, G., & Charlot, S. 2003, MNRAS, 344, 1000
Buat, V. 1992, A&A, 264, 444
Buat, V., et al. 2005, ApJ, 619, L51
Calzetti, D., Armus, L., Bohlin, R. C., Kinney, A. L., Koornneef, J., & Storchi-Bergmann, T. 2000, ApJ, 533, 682
Calzetti, D., Kinney, A. L., & Storchi-Bergmann, T. 1994, ApJ, 429, 582
Chabrier, G. 2003, PASP, 115, 763
Charlot, S., & Fall, S. M. 2000, ApJ, 539, 718
Charlot, S., Kauffmann, G., Longhetti, M., Tresse, L., White, S. D. M., Maddox, S. J., & Fall, S. M. 2002, MNRAS, 330, 876
Charlot, S., & Longhetti, M. 2001, MNRAS, 323, 887
Cortese, L., et al. 2006, ApJ, 637, 242
Erb, D. K., Shapley, A. E., Pettini, M., Steidel, C. C., Reddy, N. A., & Adelberger, K. L. 2006a, ApJ, 644, 813
Erb, D. K., Steidel, C. C., Shapley, A. E., Pettini, M., Reddy, N. A., & Adelberger, K. L. 2006b, ApJ, 647, 128
———. 2006c, ApJ, 646, 107
Heckman, T. M., et al. 2005, ApJ, 619, L35
Hoopes, C. G., et al. 2007, ApJS, 173, 441
Isobe, T., Feigelson, E. D., Akritas, M. G., & Babu, G. J. 1990, ApJ, 364, 104
Johnson, B. D., et al. 2006, ApJ, 644, L109
———. 2007, ApJS, 173, 377 (J07)
Kauffmann, G., et al. 2003a, MNRAS, 341, 33
———. 2003b, MNRAS, 341, 54
Kennicutt, R. C. Jr., 1998, ARA&A, 36, 189
Kong, X., Charlot, S., Brinchmann, J., & Fall, S. M. 2004, MNRAS, 349, 769
Kriek, M., et al. 2006a, ApJ, 645, 44
———. 2006b, ApJ, 649, L71
Kroupa, P. 2001, MNRAS, 322, 231
Marchesini, D., et al. 2007, ApJ, 656, 42
Martin, D. C., et al. 2005, ApJ, 619, L1
Meurer, G. R., Heckman, T. M., & Calzetti, D. 1999, ApJ, 521, 64
Morrissey, P., et al. 2005, ApJ, 619, L7
———. 2007, ApJS, 173, 682
Ree, C. H., et al. 2007, ApJS, 173, 607
Rudnick, G., et al. 2006, ApJ, 650, 624
Salim, S., et al. 2005, ApJ, 619, L39
———. 2007, ApJS, 173, 267 (Sa07)
Schiminovich, D., et al. 2005, ApJ, 619, L47
Seibert, M., et al. 2005, ApJ, 619, L55 (Se05)
Steidel, C. C., Adelberger, K. L., Giavalisco, M., Dickinson, M., & Pettini, M. 1999, ApJ, 519, 1
Strateva, I., et al. 2001, AJ, 122, 1861
Tremonti, C. A., et al. 2004, ApJ, 613, 898
van Dokkum, P. G., Kriek, M., Rodgers, B., Franx, M., & Puxley, P. 2005, ApJ, 622, L13
van Dokkum, P. G., et al. 2006, ApJ, 638, L59
Wang, B., & Heckman, T. M. 1996, ApJ, 457, 645
Willmer, C. N. A., et al. 2006, ApJ, 647, 853
Witt, A. N., Thronson, Jr., H. A., & Capuano, Jr., J. M. 1992, ApJ, 393, 611
Wyder, T. K., et al. 2005, ApJ, 619, L15
———. 2007, 173, 293